Hydration of Lanthanide Chloride Salts: A Quantum Chemical and Classical Molecular Dynamics Simulation Study

Cesar Beuchat,[†] Daniel Hagberg,[†] Riccardo Spezia,[‡] and Laura Gagliardi*[,§]

Department of Physical Chemistry, University of Geneva, 30 Quai Ernest Ansermet, CH-1211 Geneva, Switzerland, CNRS, Laboratoire Analyse et Modélisation pour la Biologie et l'Environnement, UMR 8587, Université d'Evry Val d'Essonne, Boulevard F. Mitterrand, 91025 Evry Cedex, France, and Department of Chemistry and Supercomputing Institute, University of Minnesota, 207 Pleasant Street SE, Minneapolis, Minnesota 55455-0431, United States

Received: June 17, 2010; Revised Manuscript Received: October 3, 2010

We present the results of a quantum chemical and classical molecular dynamics simulation study of some solutions containing chloride salts of La^{3+}, Gd^{3+}, and Er^{3+} at various concentrations (from 0.05 to 5 M), with the purpose of understanding their structure and dynamics and analyzing how the coordination varies along the lanthanide series. In the La−Cl case, nine water molecules surround the central La^{3+} cation in the first solvation shell, and chloride is present only in the second shell for all solutions but the most concentrated one (5 M). In the Gd^{3+} case, the coordination number is ∼8.6 for the two lowest concentrations (0.05 and 0.1 M), and then it decreases rapidly. In the Er^{3+} case, the coordination number is 7.4 for the two lowest concentrations (0.05 and 0.1 M), and then it decreases. The counterion Cl^- is not present in the first solvation shell in the La^{3+} case for most of the solutions, but it becomes progressively closer to the central cation in the Gd^{3+} and Er^{3+} cases, even at low concentrations.

1. Introduction

The hydration of transition metals, lanthanides, and actinides in aqueous solution is a topic that attracts the attention of many chemists, as this process is of relevance to environmental problems[1] and medicinal applications.[2] The understanding of the coordination of lanthanides (III) and the water exchange process in water solution is particularly important in relation to magnetic resonance imaging,[2] catalysis, and nuclear fuel processing.[3] Moreover, lanthanides (III) are chemical analogs of actinides (III), and understanding their hydration and complexation properties is relevant to the separation of lanthanides (III) from actinides (III).[1,4] There is also a fundamental question concerning the coordination number behavior and the three-dimensional structure across the lanthanide series.[5,6] It is well established that the Ln^{3+}−water distance decreases in an almost continuous way along the lanthanide series, and the lighter ions are predominantly nine-coordinate species, whereas the heavier ions are predominantly eight-coordinate species.[7,8] Experimentally, neutron scattering, X-ray,[5,6] extended X-ray diffraction,[9−11] extended X-ray absorption fine structure (EXAFS)[12,13] densities,[14] and spectrophotometric[15] techniques have been employed to confirm this trend. Spedding and co-workers proposed the so-called gadolinium break model to explain it.[16] Habenschuss and Spedding, by employing X-ray diffraction on $LnCl_3$ solutions, have also pointed out that the modification of the coordination number across the series does not occur through a break, but in the region between Nd^{3+} and Tb^{3+}, the solution has an average water coordination transitional between 9 and 8.[9−11] Helm, Merbach and co-workers[6,17] studied water self-exchange reactions along the series by both theory and experiment, and they could explain several of the structural and dynamical properties of these compounds. They proposed a model according to which there is not a sudden change, but rather, a progressive stabilization of the 8-fold structure with respect to the 9-fold one, identifying Eu^{3+} as the turning point, such that for this cation in solution, one should find a thermal equilibrium between the two forms, leading to a CN of 8.5.[7,18] Persson et al.,[8] based on accurate surface EXAFS analysis, have recently suggested a similar model with no sudden change in hydration number across the series, but a decrease starting at Ho^{3+}.

From a theoretical point of view, Floris and Tani[19] obtained a constant coordination number (CN) of 9 along the series and an opposite residence time behavior, performing molecular dynamics simulations with ion−water pair potentials based on ab initio calculations using a polarizable continuum model. In 2002, Cosentino et al.[20] determined molecular structures, relative stability of the octa- and nonahydrated species, and ion hydration free energies for neodymium(III) and ytterbium(III) aqueous ions using a mixed discrete continuum model. The same authors also studied the conformational behavior in aqueous solution of the EgadMe complex, a conditional gadolinium-based contrast agent sensitive to β-galactosidase enzymatic activity, by means of ab initio calculations and classical molecular dynamics simulations.[21] Clavaguera et al.[22] performed a molecular dynamics study of the hydration of La^{3+} and Eu^{3+}, including many-body effects. They showed that although La^{3+} has a prevailing CN of nine, in the Eu^{3+} case, an arrangement between CN = 9 and 8 is preferred. They emphasized that only an explicit high-level treatment of polarization effects leads to an agreement with experimental results.

More recently, Duvail et al. have developed a polarizable potential for La^{3+}−water interaction,[23] which provides a very good agreement with EXAFS data.[24,25] This approach was then extended to the whole lanthanoid series on the basis of known

* Corresponding author. E-mail: gagliard@umn.edu.
[†] University of Geneva.
[‡] Université d'Evry Val d'Essonne.
[§] University of Minnesota.

10.1021/jp105590h
Published on Web 11/05/2010

ionic radius and polarizability behavior across the series.[26] With this approach, they were able to point out the key role of water dynamics, interpreting structural data for the entire series. In particular, it was found a dynamics driven CN smooth change from light (CN = 9) to heavy (CN = 8) lanthanoids[27] consistent with the exchange mechanism proposed by Helm et al.[7] With this approach, they were able to point out the key role of water dynamics in interpreting structural data for the entire series.

Petit et al.[28] studied the first coordination sphere of La^{3+} in a highly concentrated (14 M) lithium chloride solution using a combination of classical molecular dynamics and density functional theory (DFT)-based first principle molecular dynamics. They obtained a solvation shell of La^{3+} containing 2 chloride ions and 6 water molecules. Very recently, Villa et al.[29] investigated aqueous solutions of (Nd^{3+}), (Gd^{3+}), and (Yb^{3+}) ion using ab initio-based flexible and polarizable analytical potentials in classical molecular dynamics simulations and described their thermodynamic, structural, and dynamic features. The results from the simulations were in agreement with the experimental hydration enthalpies, the Ln(III)−water radial distribution functions, and the water-exchange rates.

From the experimental side, Soderholm et al.[30] recently reported a study of a series of aqueous, constant ionic strength solutions containing 0.5 *m* Er^{3+} as a function of chloride/perchlorate ion concentration using high-energy X-ray scattering (HEXS) to probe the metal ion coordination environment. Chloride ions bind as both inner- and outer-sphere complexes. A quantitative analysis of the scattering data was used to determine stability constants that depend on whether the complexation with chloride ions adds or replaces the water molecules in the first coordination sphere. Soderholm et al.[30] concluded that the model that assumes the chloride ion adds to the water molecules in the first coordination sphere provides a better fit not only of the HEXS data but also of solvent extraction data.

The aim of the present paper is to examine the structural and dynamical behavior of aqueous solutions at different concentrations of lanthanide (III) chloride salts using quantum chemical and classical molecular dynamic simulations methods. We try to understand how the coordination structure of Ln^{3+} depends on the $LnCl_3$ salt concentration along the lanthanide series. To our knowledge, this is the first molecular dynamics simulation study using fully ab initio potentials of a system containing not only a cation in water but also the counterion.

We believe that to understand the structural and chemical behavior of highly charged systems in solution from a computational perspective, classical simulations are not sufficient. This is especially true for lanthanide and actinide ions, for which there are only limited experimental data and for which it is thus difficult to parametrize intermolecular potentials. At the same time, it is also necessary to go beyond a purely quantum chemical treatment of an ion in a polarizable continuum medium, because what is of interest is the dynamical behavior, rather than the cluster-type structure of these systems. Our approach consists of generating fully ab initio intermolecular potentials and using them in subsequent classical molecular dynamics simulations. One of the major advantages of this method is that the intermolecular potentials are, in principle, transferable from one system to another. Moreover, within our procedure, we do not need to know the experimental results in advance, from which deriving the empirical potentials. This allows the study of systems that still represent a challenge from the experimental point of view, such as lanthanide and actinide systems, for cost and safety reasons. With this, we do not mean to question the importance of semiempirical potentials; we simply would like to emphasize the different strengths of various methods. The reader should also bear in mind that in addition to heavy metals, many studies have been performed on force fields for metal cations in general, and polarizable force fields have been extensively reviewed. See, for example, refs 31 and 32.

By using the present QM/MM coupling, we have studied the coordination of uranyl in water,[33] showing that five water molecules coordinate around uranyl in the first shell, with a U−O (water) bond distance of 2.40 Å, in agreement with experiments. A second coordination shell was predicted to be at a distance of 4.7 Å from the central uranyl. We have also performed molecular dynamics simulations of Cm^{3+} in water[34] at two different temperatures; namely, $T = 300$ and 473 K. At the lower temperature, $T = 300$ K, nine water molecules coordinate preferentially to the Cm^{3+} ion in the first coordination sphere, but at the higher temperature, $T = 473$ K, the coordination number shifts toward eight.

In the present study, we consider aqueous solutions of three lanthanide ion chloride salts, namely $LaCl_3$, $GdCl_3$, and $ErCl_3$ at various concentrations. We have chosen these three cations because they are, respectively, at the beginning, in the middle and toward the end of the lanthanide series and they are representative of the changes that occur along the series.

The paper is organized as follows: In Section 2, we describe the computational details. In Section 3, we report the results of the simulations and their discussion. Finally, in Section 4, some conclusions are presented.

2. Computational Details

All quantum chemical calculations were performed with the software MOLCAS-7.2.[35] The complete active space (CAS) SCF method[36] was used to generate molecular orbitals and reference functions for subsequent multiconfigurational, second-order perturbation calculations of the dynamic correlation energy (CASPT2).[37]

Scalar relativistic effects were included using the Douglas−Kroll−Hess Hamiltonian and relativistic ANO-RCC basis sets[38] of VQZP quality. In the CASSCF calculations, the active space was formed by the Ln 4f orbitals. In the La^{3+} case, corresponding to the valence electronic configuration $4f^0$, the active space was thus empty, and the calculation was reduced to a conventional Hartree−Fock followed by perturbation theory to second order, MP2, calculation. In the Gd^{3+} case, we considered the $^8S_{7/2}$ ground state corresponding to the valence electronic configuration $4f^7$. In the Er^{3+} case, we considered the $^4I_{3/2}$ quartet ground state, corresponding to the valence electronic configuration $4f^{11}$. The combination of the CASSCF/CASPT2 approach with ANO-RCC basis sets has been successful in studying many actinide- and lanthanide-containing systems.[38−47]

The structure of the water molecule was optimized using Møller−Plesset second-order perturbation theory (MP2). The intermolecular potential energy curves between Ln^{3+}−Ln^{3+}, Ln^{3+}−Cl^-, and Ln^{3+}−water were generated at the CASPT2 level of theory (MP2 in the La^{3+} case), including basis set superposition energy (BSSE) corrections with the counterpoise method.[48] The Cl^-−water, Cl^-−Cl^-, and water−water potentials were generated at the MP2 level of theory. For the supermolecular systems, Ln^{3+} plus water and Ln^{3+} plus Cl^-, the active space in the CASSCF calculation was the same as in the isolated Ln^{3+} cases (in the La^{3+} case, the active space was empty, which is equivalent to a Hartree−Fock calculation) while the occupied molecular orbitals of water (and Cl^-) were kept inactive.

TABLE 1: The Fitted Parameters for the Various Potentials

	K^{ct}	K^{ere}	a^{ct}	a^{ere}		K^{ere}	a^{ere}
La−O	4 165	202 607	1.526	2.861	La−H	544 051	7.027
Gd−O	28 006	101 852	1.777	2.270	Gd−H	273 498	4.182
Er−O	11 656	307 627	2.109	3.251	Er−H	826 056	8.788
La−Cl	206 426	288 201	1.529	1.633	Cl−O	1 600 999	8.801
Gd−Cl	210 922	347 269	1.636	1.812	Cl−H	596 220	3.552
Er−Cl	197 022	364 743	1.742	1.957			

See eq 2. K is expressed in kJ/mol, and a, in Å^{-1}.

The intermolecular potential used in the simulations was constructed using the NEMO procedure,[49] according to which the total interaction energy is written as the sum of five terms:

$$E^{tot} = E^{ele} + E^{ind} + E^{disp} + E^{ere} + E^{ct} \quad (1)$$

The starting point for the construction of a NEMO potential is one quantum chemical calculation on each of the interacting subsystems. From the wave function of the subsystems, a distributed set of charges, dipoles, and quadrupoles are calculated for each of the atoms (although the quadrupoles are replaced by dipoles on atoms close to the site for the quadrupole in the actual simulations).[50] Local polarizabilities are calculated from the wave function using perturbation theory.[51] Local multipoles and polarizabilities are used to estimate the electrostatic, E^{ele}, and induction interaction, E^{ind}, between the two subsystems. The dispersion interaction, E^{disp}, is calculated using a London-type formula.[49] To determine the last two terms in eq 1 (the exchange repulsion energy, E^{ere}, and charge transfer energy, E^{ct}), the contributions from the first three terms in eq 1 are subtracted from the total interaction energy between the two subsystems.

The sum of these two terms, $E^{ere} + E^{ct}$, is then fitted as a sum of interatomic exponential terms, which is used for the final construction of the NEMO potential.

$$E^{ere} + E^{ct} = \sum_{i,j} \left(K_{ij}^{ere} e^{-a_{ij}^{ere} r_{ij}}\right) - K_{LnO}^{ct} e^{-a_{LnO}^{ct} r_{LnO}} - K_{LnCl}^{ct} e^{-a_{LnCl}^{ct} r_{LnCl}} \quad (2)$$

The first term describes E^{ere}, and r_{ij} represents the distance between atoms i and j. The sum runs over all interacting atom pairs i, j. The second and third, attractive, terms describe the charge transfer, occurring only between the Ln^{3+} ion and the water oxygen and between the Ln^{3+} ion and the Cl^- ion. The fitting parameters for the various species are reported in Table 1. For the water−water potentials, the same repulsion parameters were used as those reported in ref 33.

Preliminary results of the calculations of the ab initio Ln^{3+}−H_2O intermolecular potentials showed that an electron transfer occurs between the H_2O molecule and the Ln^{3+} at large separation (∼10 Å apart). This means that in the gas phase, the right-hand side of the equilibrium

$$Ln^{3+} + H_2O \leftrightarrow Ln^{2+} + H_2O^+$$

is favored. One can easily demonstrate it by simple inspection of ionization potentials of Ln. So instead of having Ln^{3+} and H_2O, one has Ln^{2+} and H_2O^+. The same situation occurs in the equilibrium

$$Ln^{3+} + Cl^- \leftrightarrow Ln^{2+} + Cl$$

One can easily demonstrate that the right-hand side of this equilibrium is favored by simple inspection of the ionization potential of Ln and the electron affinity of Cl.

The only way to favor the left-hand side of these equilibria (the more ionic species) is to solvate the ions by a sufficient number of explicit water molecules in the subsystems. After extensive testing, we have found that the left-hand sides are favored for the following reactions:

$$Ln^{3+}\cdot H_2O + H_2O \leftrightarrow Ln^{2+}\cdot H_2O + H_2O^+$$

$$Ln^{3+}\cdot 6H_2O + Cl^-\cdot 4H_2O \leftrightarrow Ln^{2+}\cdot 6H_2O + Cl\cdot 4H_2O$$

and we have thus generated intermolecular potentials between the following subsystems:

$$Ln^{3+}\cdot H_2O \text{ and } H_2O$$

$$Ln^{3+}\cdot 6H_2O \text{ and } Cl^-\cdot 4H_2O$$

The distance between the various atoms/molecules in each subsystem was optimized and kept fixed while generating the intermolecular potential between the two subsystems.

One point of concern is whether the results depend on the way in which the various potentials are generated. The Ln−H_2O and Ln−Cl potentials should be built with the smallest possible number of water molecules around Ln to not include many-body polarization terms in the potential. But if too few water molecules are considered, the Ln^{3+} is reduced to Ln^{2+}. The various curves are reported in either the tables or figures of the Supporting Information.

This is not unexpected, since the importance of charge transfer in metal−water interactions in gas phase is well-known,[52,53] and the subsequent Coulomb repulsion is the physical basis of instability of multiply charged hydrated ions in the gas phase.[54−60] A complete description of such a problem would require a treatment that goes beyond the Born−Oppenheimer approximation. However, this is not necessary in the liquid phase, where charge transfer plays a minor role. The role of charge transfer is known to decrease in clusters with an increasing number of water molecules.[52,61] An analogue decreasing of charge transfer as a function of the number of water molecules was recently described in the polarizable AMOEBA force field developed for Zn^{2+} in water.[62]

In the Ln−water case, we can reduce to one the number of additional water molecules around the Ln ion to avoid relevant charge transfer effects. In the Ln−Cl case, we were forced to include six water molecules around the Ln ion to avoid charge transfer taking place. We assume in this case that many-body effects are small with respect to the total interaction energy. This can be justified by the predominance of charge−charge interactions between triply positively charged Ln^{3+} and negatively charged Cl^-.

All molecular dynamics simulations were performed using the Molsim package.[63] Seven solutions at different concentrations of the salts were studied: namely, 0.05, 0.10, 0.20, 0.50, 1.00, 2.00, and 5.00 M at a constant temperature of 300 K. Two boundary conditions were chosen for the simulations: the droplet and periodic boundary condition (PBC).

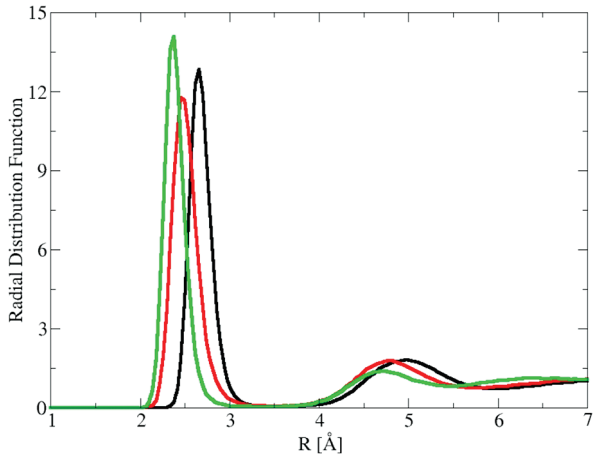

Figure 1. Radial distribution functions between Ln^{3+} and the water oxygen for the 0.05 M solutions. Black, La^{3+}; red, Gd^{3+}; green, Er^{3+}.

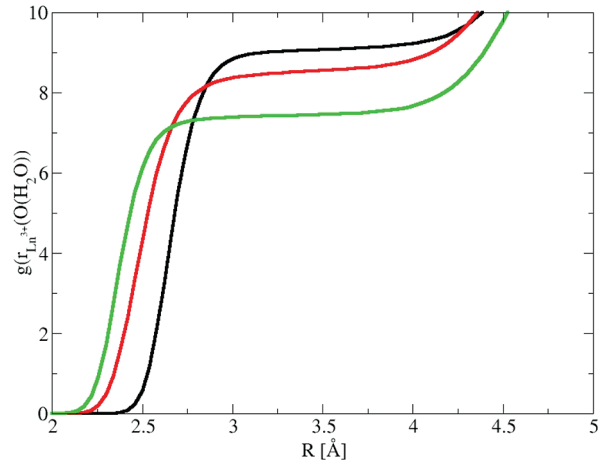

Figure 2. Coordination number of water around Ln^{3+} for the 0.05 M solutions. Black, La^{3+}; red, Gd^{3+}; green, Er^{3+}.

The boundary conditions for the droplet consist in a weak, spherical potential that prevents the molecules and ions from drifting away. It also prevents the droplet from deforming substantially. This external potential starts acting at a distance of 20 Å, and it has the functional form $0.1(r - 20)^2$ kJ/mol, where r is the distance from the origin (we subtract 20 because this is the diameter of the droplet). The same approach was previously used for the Cm^{3+} ion in a water droplet.[34]

For the periodic boundary conditions, a standard Ewald simulation with a box length of 32.23 Å was performed. The setup of the Ewald parameters was done according to Kolafa's prescription[64] with a radial cutoff equal to 15 Å, and the tolerance was set to 0.01 kJ/mol. The number of particles in the system, 1120, which was kept constant in all simulations, corresponds to the volume of a droplet with a radius of 20 Å.

Molecular dynamics simulations were performed on various droplets with concentrations equal to 0.05, 0.10, 0.20, 0.50, and 1.00 M, respectively. Periodic boundary condition, PBC, simulations were performed for concentrations of 0.50, 1.00, 2.00, and 5.00 M. The equilibration time was equal to 0.1 ns, and the production time was equal to 1 ns. In the following, we will show that the two methods give similar results, in particular, concerning Ln−O distances and structure. Small differences are found for the Ln−Cl structure, but largely inside thermal fluctuations. It is quite expected that PBC and droplet methods provide similar structural results,[65,66] and solvation free energy can differ substantially.[67] In particular, recent studies of free energy calculations using both PBC[68,69] and droplet[70,71] methods showed that there is no clear trend in what is preferable. Note that PBC simulations of our systems are, on average, 30% slower than droplet ones, and thus, since structural features are similar in the two methods, we will report in the following the study of the full concentration range as obtained by the droplet method.

3. Results and Discussion

We start by presenting the structural results at low concentration. In Figures 1 and 2, the radial distribution functions (RDF) between Ln^{3+} and the water oxygen for the 0.05 M solutions and the corresponding coordination numbers are reported. The Ln−O distance decreases along the Ln series. In the La^{3+} case, the first and second peaks are centered at 2.66 and 4.98 Å, respectively, but in the Gd^{3+} case at 2.48 and 4.78 Å, respectively, and in the Er^{3+} case at 2.37 and 4.70 Å, respectively. The CN decreases along the series, in agreement with earlier

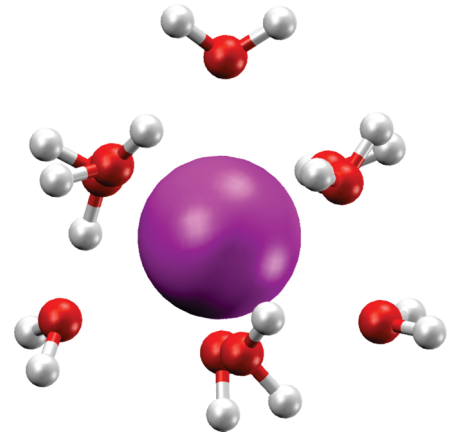

Figure 3. A snapshot of the first shell of water molecules around La^{3+} in a tricapped trigonal prism arrangement.

results.[27] The La^{3+} ion presents an average CN of 9.1 water molecules in the first shell (Figure 3) and an average CN of 19.1 in the second shell. From the O−Ln−O angular distribution function (ADF) of the first hydration shell, we obtain some information on (i) the structure from the peak positions and (ii) the thermal fluctuation from their width, reflecting the underlying dynamics. Since we do not have a single conformation, it is not possible to identify a unique symmetry of the system. More realistically, the overall symmetry derives from some dynamical averaging. In the case of La^{3+}, ADF shows two peaks corresponding to a tricapped trigonal prism (TTP) first hydration structure (Figure 4). This shape is similar to what found by previous classical[26,72,73] and DFT-based[74] molecular dynamics simulations in liquid water.

Further, by decomposing La−O radial distribution function of 9-fold structures into two Gaussian distributions, we found two subpopulations: one composed of 5−6 water molecules at a short distance (in a 2.61−2.65 Å range) and another composed by 3−4 water molecules at a longer distance (at ∼2.77 Å). Details of this decomposition are shown in the Supporting Information. This corresponds to a TTP structure[8] that dynamically interconverts but where prismatic and equatorial water molecules are distinguishable. Similar results were found in other simulations.[26,74] On the other hand, Floris and Tani[19] found a larger difference between shorter (prismatic) and longer (equatorial) distances and a coexistence of TTP and capped square antiprism structures. Note that the liquid phase seems to be a key ingredient to ensure a 6 + 3 structure in which the

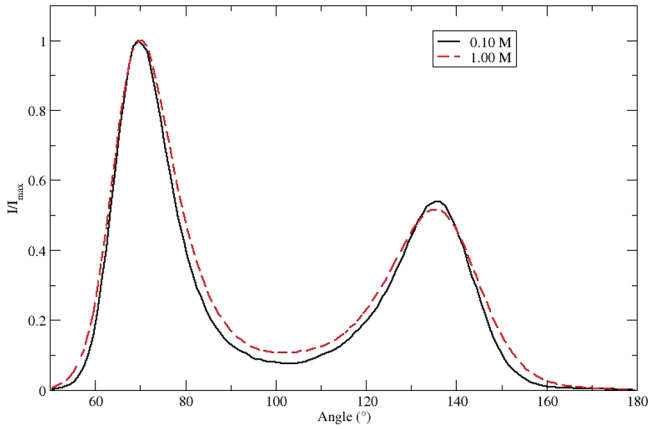

Figure 4. Angular distribution functions of O−La−O in the first hydration shell at different concentrations.

prismatic water molecules are at a distance that is ∼0.1 Å shorter than equatorial ones. In fact, MP2 and DFT calculations done in vacuum predict a smaller distance or even, in a few cases, equatorial water molecules at a slighter shorter distance than the prismatic one.[75,76]

Gd^{3+} has an average CN of 8.6 water molecules in the first shell and 15.2 in the second shell. Er^{3+} is surrounded by 7.4 water molecules in the first shell and 11.1 in the second shell, in agreement with experimental values (8 water molecules in the first shell and 9−12 in the second shell).[30] In the Er^{3+} case, the ADF (Figure 9) has a shape that corresponds better to a square antiprism structure.

The Ln−Cl distance decreases along the series: the La−Cl peak is centered at 4.2 Å; the Gd−Cl peak, at 3.7 Å; and the Er−Cl peak, at 3.1 Å, respectively. This means that Cl^- gradually approaches the first hydration shell: in the La^{3+} case, Cl^- is at a position roughly corresponding to the second hydration shell; in the Gd^{3+} case, Cl^- is closer than the main Gd−O second shell peak; in the Er^{3+} case, Cl^- resides between the first and second water hydration shells. In this case, Cl^- is placed at a distance that does not allow any water molecule to be between the anion and the cation. We can thus consider it in a "far" first hydration shell, where by "far" we mean that it is not a standard first shell.

The structural behavior of the systems under examination varies with the salt concentration. In Table 2, the CNs and RDF peak positions of water and chloride around the three Ln^{3+} ions are reported for different concentrations. We also report the full weight at half-maximum (fwhm) of first and second RDF peaks and associated statistical confidence for CNs. For La^{3+}, the water CN is similar for all concentrations, except for the 5.0 M solution, in which a drastic change in the first coordination shell occurs and one Cl^- ion replaces two water molecules. One should bear in mind that 5.0 M corresponds to an oversaturated solution, since the solubility of this salt is ∼4 M. This behavior should be compared with that found by Petit et al.,[28] even if their chemical conditions were different from ours. In their case, they worked with a 14 M lithium chloride solution and obtained a solvation shell of La^{3+} containing 2 chloride ions and 6 water molecules. For Gd^{3+}, there are 8.6 water molecules in the first shell for the two lowest chloride ion concentrations (0.05 and 0.10 M), similarly to what found in other simulations in which only the cation is present,[27,29] thus mimicking "ideal dilution". Then the water CN number decreases already for the 0.2 M solution. Figure 6 shows the decrease of the Gd^{3+}−O distance as an effect of the increase of concentration. For Er^{3+}, the presence of Cl^- has an effect on water CN also at low concentrations. In fact, it is 7.4 for the two lowest concentrations, and then it decreases to 6.

One should notice that concentration has basically no effect on fwhm of the first peak La−O RDF, but it has a small effect on the second peak La−O RDF (it slightly increases with concentration). On the other hand, fwhm of Ln−Cl RDF increases significantly with concentration, ∼0.6 Å for La^{3+}, where Cl^- interacts less, and ∼1 Å for Gd^{3+} and Er^{3+}, where it interacts more. Statistical fluctuations of CNs depend on the

TABLE 2: RDF for First and Second Peak Positions, in Å, and CNs of Water (first and second shell) and Chloride (first shell) around Ln^{3+} for Different Concentrations [M][a]

concn	RDF peak (Å)	CN	RDF peak (Å)	CN	RDF peak (Å)	CN
	La−O(first shell)		La−O(second shell)		La−Cl	
0.05	2.66 (0.27)	9.1 (0.3)	5.0 (1.1)	19.1 (1.9)	4.2 (0.5)	0.0 (0)
0.10	2.66 (0.26)	9.1 (0.3)	5.0 (1.1)	19.6 (1.9)	4.3 (0.5)	0.0 (0)
0.20	2.65 (0.28)	9.0 (0.3)	5.0 (1.1)	18.0 (2.6)	4.2 (0.6)	0.0 (0)
0.50	2.63 (0.29)	8.9 (0.5)	5.1 (1.3)	19.1 (2.5)	4.3 (0.7)	0.0 (0)
1.00	2.62 (0.29)	8.9 (0.9)	5.1 (1.5)	18.3 (2.9)	4.3 (0.7)	0.0 (0)
2.00	2.58 (0.28)	8.8 (0.6)	5.1 (1.8)	18.9 (2.8)	4.3 (0.7)	0.2 (0.1)
5.00	2.54 (0.27)	7.9 (1.1)	5.2 (1.9)	15.8 (3.7)	2.9 (1.1)	0.8 (0.7)
concn	Gd−O(first shell)		Gd−O(second shell)		Gd−Cl	
0.05	2.48 (0.31)	8.6 (0.5)	4.8 (0.9)	15.2 (1.8)	3.7 (0.8)	0.3 (0.5)
0.10	2.44 (0.33)	8.3 (0.6)	4.9 (0.9)	14.3 (2.2)	4.0 (0.9)	0.8 (0.8)
0.20	2.41 (0.34)	7.6 (0.8)	4.9 (1.3)	14.0 (2.3)	3.9 (1.0)	1.0 (0.9)
0.50	2.39 (0.35)	7.5 (1.0)	5.0 (1.4)	14.8 (2.4)	3.9 (1.7)	1.2 (1.1)
1.00	2.38 (0.35)	7.0 (1.2)	5.1 (1.6)	15.0 (2.2)	4.0 (1.8)	1.7 (1.5)
	Er−O(first shell)		Er−O(second shell)		Er−Cl	
0.05	2.38 (0.25)	7.4 (0.7)	4.7 (1.0)	11.1 (2.5)	3.1 (0.4)	1.0 (0.7)
0.10	2.38 (0.27)	7.4 (0.8)	4.8 (1.1)	12.2 (2.6)	3.1 (0.8)	0.6 (0.7)
0.20	2.31 (0.27)	6.8 (0.7)	4.7 (1.0)	11.0 (2.4)	3.3 (1.0)	0.7 (0.7)
0.50	2.27 (0.25)	6.0 (1.0)	4.9 (1.5)	11.1 (2.5)	3.1 (1.3)	1.3 (1.2)
1.00	2.27 (0.24)	6.1 (1.0)	4.9 (1.5)	10.9 (2.6)	3.3 (1.5)	1.1 (1.2)

[a] We defined the first and second hydration shell from the minima in RDF; that is, 3.5 (La^{3+} and Gd^{3+}) and 3.3 (Er^{3+}) for the first shell and 3.5−6.1 (La^{3+}), 3.5−5.7 (Gd^{3+}) and 3.3−5.5 (Er^{3+}) for the second shell. In parentheses, we show full weight at half maximum, fwhm, of RDF first and second peaks and statistical fluctuations of CNs.

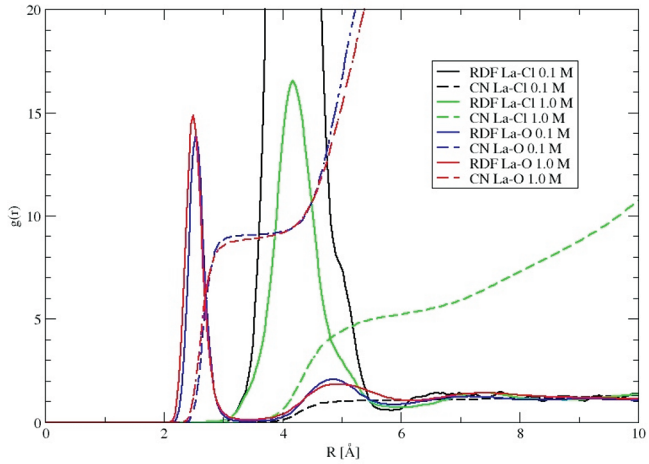

Figure 5. RDFs and CNs of water and chloride around La^{3+} for different concentrations.

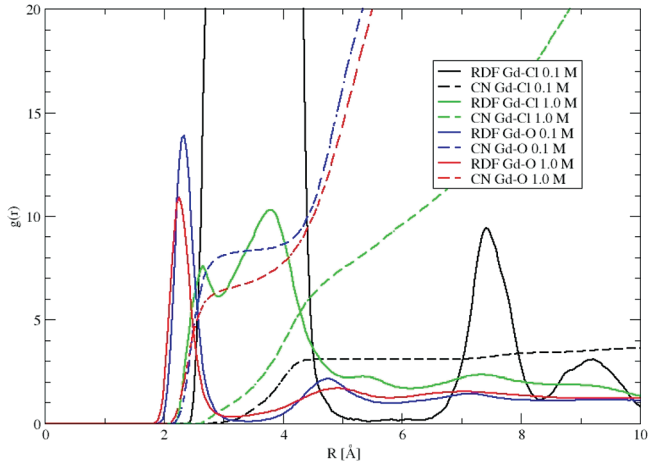

Figure 6. RDFs and CNs of water and chloride around Gd^{3+} for different concentrations.

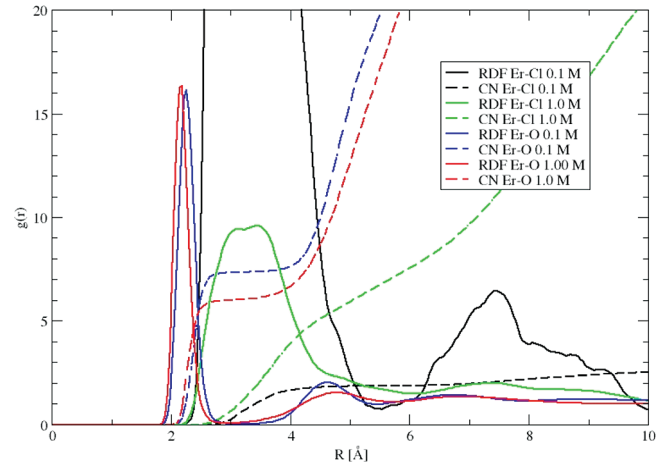

Figure 7. RDFs and CNs of water and chloride around Er^{3+} for various concentrations.

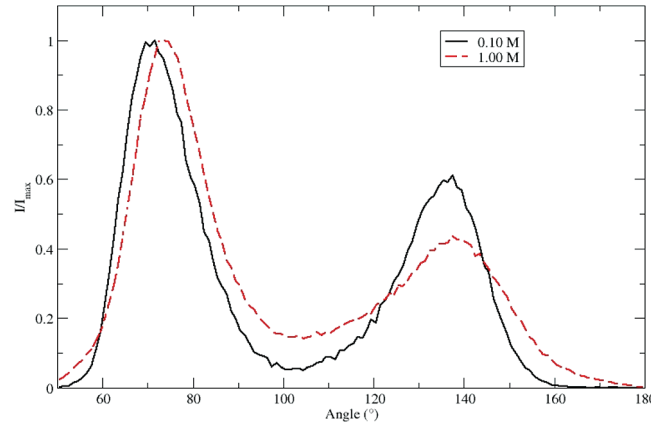

Figure 8. ADFs of O−Gd−O in the first hydration shell at different concentrations.

concentration. They increase with concentration, in particular for the first shell. This reflects the fact that at higher concentrations, Cl^- interacts with Ln^{3+}, and thus, it affects the first shell water dynamics. As a consequence, second hydration shell CNs statistical fluctuations are less affected by concentration, except in the case of La^{3+}, where there is a larger change in the first shell solvation structure at high concentrations (from absolutely no Cl^- present to the incoming of about one Cl^- into the vicinity of La^{3+}).

In Table 3, we report the percentage of various coordination numbers for different concentrations of the La, Gd, and Er salts.

For La^{3+}, at lower concentrations, 0.05−0.2 M, the second most probable coordination number after 9 is 10, but at higher concentrations, 0.5−1.0 M, the second most probable coordination number becomes 8. The behavior at low concentration is similar to the one observed by Duvail, et al.,[23] and the behavior at higher concentration has similarities with the one proposed by Helm and Merbarch for the $Nd(H_2O)_9^{3+}/Nd(H_2O)_8^{3+}$ system.[7] For Gd^{3+}, at lower concentration, 0.05 M, the most probable coordination number is 9. For the 0.1, 0.2, and 0.5 M solutions, the most probable CN is 8, and the second probable stoichiometry is 9 at lower concentrations and 7 at higher concentrations. For the 1 M solution, the most probable CN is 7. This confirms the trend we observed in which the 7-fold structure is progressively stabilized as the concentration increases. In the Er^{3+} case, the most probable CN is equal to 8 for the 0.05 and 0.1 M solutions, whereas for the 0.2, 0.5, and 1 M solutions, it is equal to 7. This effect of the concentration could also be observed by the change of the shape in the ADF (Figures 8 and 9).

In the Gd^{3+} case, Cl^- is present in the first solvation shell already at 0.5 M concentration. In the Er^{3+} case, Cl^- is present in the first solvation shell at even lower concentrations. This trend in going from La^{3+} to Gd^{3+} to Er^{3+} reflects the contraction of the lanthanide radius and the $Ln^{3+}-Cl^-$ distance along the series. In Figures 5−7, we report the radial distribution functions

TABLE 3: Percentage of Different Coordination Numbers, For Various Concentrations of the La, Gd, and Er Salts

	La			Gd			Er		
concn, M	CN = 8	CN = 9	CN = 10	CN = 7	CN = 8	CN = 9	CN = 6	CN = 7	CN = 8
0.05	1.5	91.0	7.5	0.3	39.7	60.0	9.3	39.5	51.2
0.1	1.7	89.5	8.8	5.0	56.6	38.0	20.6	22.1	56.7
0.2	4.7	88.0	7.2	26.2	55.2	9.0	36.9	48.1	14.4
0.5	14.0	78.5	7.3	29.4	47.8	11.4	14.6	46.0	27.1
1.0	19.8	75.1	5.7	38.3	31.8	4.2	13.0	46.5	28.5

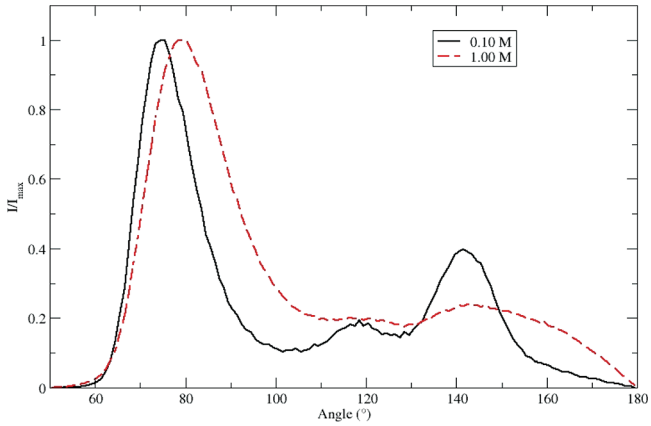

Figure 9. ADFs of O−Er−O in the first hydration shell at different concentrations.

and coordination number of Cl^- and O around the three cations at various concentrations to show the relative position of Cl^- during the simulation. It is interesting to compare our results to the recent Er^{3+} experiment by Soderholm et al.,[30] according to which the chloride adds to, and does not replace, the waters in the first coordination sphere. On the basis of our simulation at a concentration of 0.05 M, the average coordination number for water molecules is 7.4 (with a statistical fluctuation of 0.7), and there is a 90% probability of finding at least one chloride in the first (or second) solvation shell. A first hydration shell with an average CN of 7.4 derives from the statistical coexistence of different CNs, as reported in Table 3. We can have 8 coordinated waters and 1 chloride lying on the sphere (the Er−Cl rdf peak is at 3.1 Å, and the first shell radius is 3.3 Å) with an observed probability of 51.2%. However, we also have a not negligible probability (39.5%) for one chloride and only 7 waters around erbium. A smaller probability (9.3%) is associated with 6 water molecules around erbium, thus giving the overall CN of 7.4. We can thus say that an equilibrium occurs between the 8 waters + 1 chloride and 7 waters + 1 chloride conformations, where the Cl^- is systematically at a longer distance. Increasing the concentration has the effect of stabilizing the 7 waters + 1chloride conformation.

In Figure 9, we report the ADFs of oxygen around Er^{3+} at two different concentrations, from which we can observe the change in conformation due to the presence of the chloride anion. However, the trend observed in our calculations seems to contradict the EXAFS results of Allen, et al.,[77] who observed a decrease in $Ln^{3+}-Cl^-$ ion complexation in the first coordination sphere going across the series and not much change in the total coordination number (although with a large uncertainty in this number). Their data showing Cl^- ion complexation were obtained at 14 M LiCl which, because the water activity is drastically lowered, might not be directly comparable. They observed no Cl^- ion complexation at 0.25 M LiCl for the La^{3+}, Ce^{3+}, Nd^{3+}, Eu^{3+}, and Yb^{3+} ions.[77]

We observe the same trend for the Ln−Cl distance. Notice that CN determined by EXAFS can have a large uncertainty, depending on the fitting procedure. In their case, for example, the Ln−water coordination number is stable across the series, whereas other experiments and simulations show a decrease in the water CN across the series.[7,8,27,29] Our results are also not in agreement with previous simulation done by Ruas and co-workers[78] on $DyCl_3$. In their simulations, they did not observe even at high concentration (3.1 mol/kg) any chloride complexing the Dysprosium, but only staying in the second solvation shell. They also observed that a starting $DyCl_3$ structure did not lead to an association of chloride with the cation.

4. Conclusions

In this paper, we showed that, by using molecular dynamics techniques based on fully ab initio intermolecular potentials, it is possible to analyze the structural behavior of lanthinide ion salts in aqueous solutions. We considered aqueous solutions containing chloride salts of La^{3+}, Gd^{3+}, and Er^{3+} at various concentrations (from 0.05 to 5 M). In the La−Cl case, nine water molecules surround the central La^{3+} cation in the first solvation shell, and chloride is present only in the second shell for all solutions but the most concentrated one (5 M). In the Gd^{3+} case, the coordination number is ∼8.6 for the two lowest concentrations (0.05 and 0.1 M), and then it decreases rapidly. In the Er^{3+} case, the coordination number is 7.4 for the two lowest concentrations (0.05 and 0.1 M), and then it decreases. The different behavior of the three cations reflects the radius decrease along the series, which, according to our simulations, occurs in a smooth way and not with a sudden break in the middle of the series. We especially focused on the Er^{3+} case, the least experimentally studied of the three systems. Our results confirm the scheme recently proposed by Soderholm et al.,[30] according to which the chloride adds to, and does not replace, the waters in the first coordination sphere. Our structural data show that Cl^- comes close to Er^{3+} but at a distance that is quite considerably larger than the Ln−water one, such that the process proposed by Soderholm and co-workers[30] can sterically take place. Our approach to generate intermolecular potentials is of general validity and can be used for highly charged ions of species that are difficult to handle in a laboratory, such as lanthanide and actinide compounds.

Acknowledgment. We thank Norman M. Edelstein, Lawrence Berkeley National Laboratory; Gunnar Karlström, Lund University; and Lothar Helm, EPFL, for useful discussions. This work was supported by the Swiss National Science Foundation (Grant no. 200020-120007) and by the US Department o Energy (Grant no. USDOE/DE-SC002183).

Supporting Information Available: Supporting Information including Cartesian coordinates, intermolecular potentials, and Gaussian fits of La−O RDF first peak for different concentrations. This material is available free of charge via the Internet at http://pubs.acs.org.

References and Notes

(1) Silva, R.; Bidoglio, G.; Rand, M.; Robouch, P.; Wanner, H.; Puigdomenech, I. *Chemical Thermodynamics of Americium OECD*;: Paris, 2004.

(2) Merbach, A. E.; Tóth, É. *The Chemistry of Contrast Agents in Medical Magnetic Resonance Imaging*; John Wiley & Sons: Chichester, 2001.

(3) Nash, K. L.; Madic, C.; Mathur, J. N. Actinide Separation Science and Technology. In *The Chemistry of the Actinide and Transactinide Elements*; Morss, L. R.; Edelstein, N. M.; Fuger, J., Eds.; Springer: Dordrecht, 2006.

(4) Vitorge, P.; Phrommavanh, V.; Siboulet, B.; You, D.; Vercouter, T.; Descostes, M.; Marsden, C. J.; Beaucaire, C.; Gaudet, J. P. *C. R. Chim.* **2007**, *10* (10−11), 978–993.

(5) Cossy, C.; Barnes, A. C.; Enderby, J. E.; Merbach, A. E. *J. Chem. Phys.* **1989**, *90* (6), 3254–3260.

(6) Helm, L.; Merbach, A. E. *Structure and Dynamics of Lanthanide(III) Ions in Solution—a Neutron-Scattering Contribution*; 1991, 245−250.

(7) Helm, L.; Merbach, A. E. *Chem. Rev.* **2005**, *105* (6), 1923–1959.

(8) Persson, I.; D'Angelo, P.; De Panfilis, S.; Sandstrom, M.; Eriksson, L. *Chem.—Eur. J.* **2008**, *14* (10), 3056–3066.

(9) Habenschuss, A.; Spedding, F. H. *J. Chem. Phys.* **1979**, *70* (8), 3758–3763.
(10) Habenschuss, A.; Spedding, F. H. *J. Chem. Phys.* **1979**, *70* (6), 2797–2806.
(11) Habenschuss, A.; Spedding, F. H. *J. Chem. Phys.* **1980**, *73* (1), 442–450.
(12) Yamaguchi, T.; Nomura, M.; Wakita, H.; Ohtaki, H. *J. Chem. Phys.* **1988**, *89* (8), 5153–5159.
(13) Fox, A. R.; Bart, S. C.; Meyer, K.; Cummins, C. C. *Nature* **2008**, *455* (7211), 341–349.
(14) Spedding, F. H.; Shiers, L. E.; Brown, M. A.; Baker, J. L.; Guitierrez, L.; McDowell, L. S.; Habenschuss, A. *J. Phys. Chem.* **1975**, *79* (11), 1087–1096.
(15) Miyakawa, K.; Kaizu, Y.; Kobayashi, H. *J. Chem. Soc., Faraday Trans. I* **1988**, *84*, 1517–1529.
(16) Spedding, F. H.; Pikal, M. J.; Ayers, B. O. *J. Phys. Chem.* **1966**, *70*, 2440.
(17) Cossy, C.; Helm, L.; Powell, D. H.; Merbach, A. E. *New J. Chem.* **1995**, *19* (1), 27–35.
(18) Helm, L.; Merbach, A. E. *Coord. Chem. Rev.* **1999**, *187*, 151–181.
(19) Floris, F. M.; Tani, A. *J. Chem. Phys.* **2001**, *115* (10), 4750–4765.
(20) Cosentino, U.; Villa, A.; Pitea, D.; Moro, G.; Barone, V. *J. Phys. Chem. B* **2000**, *104* (33), 8001–8007.
(21) Cosentino, U.; Pitea, D.; Moro, G.; Saracino, G. A. A.; Villa, A. *Phys. Chem. Chem. Phys.* **2009**, *11* (20), 3943–3950.
(22) Clavaguera, C.; Pollet, R.; Soudan, J. M.; Brenner, V.; Dognon, J. P. *J. Phys. Chem. B* **2005**, *109* (16), 7614–7616.
(23) Duvail, M.; Souaille, M.; Spezia, R.; Cartailler, T.; Vitorge, P. *J. Chem. Phys.* **2007**, *127* (3), 034503.
(24) Duvail, M.; D'Angelo, P.; Gaigeot, M. P.; Vitorge, P.; Spezia, R. *Radiochim. Acta* **2009**, *97* (7), 339–346.
(25) Spezia, R.; Duvail, M.; Vitorge, P.; D'Angelo, P. *J. Phys.: Conf. Series* **2009**, *190*, 012056.
(26) Duvail, M.; Vitorge, P.; Spezia, R. *J. Chem. Phys.* **2009**, *130*, 104501.
(27) Duvail, M.; Spezia, R.; Vitorge, P. *ChemPhysChem* **2008**, *9* (5), 693–696.
(28) Petit, L.; Vuilleumier, R.; Maldivi, P.; Adamo, C. *J. Phys. Chem. B* **2008**, *112* (34), 10603–10607.
(29) Villa, A.; Hess, B.; Saint-Martin, H. *J. Phys. Chem. B* **2009**, *113* (20), 7270–7281.
(30) Soderholm, L.; Skanthakumar, S.; Wilson, R. E. *J. Phys. Chem. A* **2009**, *113* (22), 6391–6397.
(31) Ponder, J. W.; Wu, C. J.; Ren, P. Y.; Pande, V. S.; Chodera, J. D.; Schnieders, M. J.; Haque, I.; Mobley, D. L.; Lambrecht, D. S.; DiStasio, R. A.; Head-Gordon, M.; Clark, G. N. I.; Johnson, M. E.; Head-Gordon, T. *J. Phys. Chem. B* **2010**, *114* (8), 2549–2564.
(32) Gresh, N.; Cisneros, G. A.; Darden, T. A.; Piquemal, J. P. *J. Chem. Theory Comput.* **2007**, *3* (6), 1960–1986.
(33) Hagberg, D.; Karlstrom, G.; Roos, B. O.; Gagliardi, L. *J. Am. Chem. Soc.* **2005**, *127* (41), 14250–14256.
(34) Hagberg, D.; Bednarz, E.; Edelstein, N. E.; Gagliardi, L. *J. Am. Chem. Soc.* **2007**, *129* (46), 14136–14137.
(35) Karlström, G.; Lindh, R.; Malmqvist, P.-Å.; Roos, B. O.; Ryde, U.; Veryazov, V.; Widmark, P.-O.; Cossi, M.; Schimmelpfennig, B.; Neogrady, P.; Seijo, L. *Comput. Mater. Sci.* **2003**, *287*, 222–239.
(36) Roos, B. O.; Taylor, P. R.; Siegbahn, P. E. M. *Chem. Phys.* **1980**, *48* (2), 157–173.
(37) Andersson, K.; Malmqvist, P.-Å.; Roos, B. O. *J. Chem. Phys.* **1992**, *96* (2), 1218–1226.
(38) Gagliardi, L.; Heaven, M. C.; Krogh, J. W.; Roos, B. O. *J. Am. Chem. Soc.* **2005**, *127* (1), 86–91.
(39) Gagliardi, L. *J. Am. Chem. Soc.* **2003**, *125*, 7504–7505.
(40) Gagliardi, L. *Theor. Chem. Acc.* **2006**, *116* (1−3), 307–315.
(41) Gagliardi, L.; Cramer, C. J. *Inorg. Chem.* **2006**, *45* (23), 9442–9447.
(42) Gagliardi, L.; La Manna, G.; Roos, B. O. *Faraday Discuss.* **2003**, *124*, 63–68.
(43) Gagliardi, L.; Pyykko, P.; Roos, B. O. *Phys. Chem. Chem. Phys.* **2005**, *7* (12), 2415–2417.
(44) Gagliardi, L.; Roos, B. O. *Chem. Soc. Rev.* **2007**, *36* (6), 893–903.
(45) Infante, I.; Gagliardi, L.; Scuseria, G. E. *J. Am. Chem. Soc.* **2008**, *130* (23), 7459–7465.
(46) Infante, I.; Gagliardi, L.; Wang, X. F.; Andrews, L. *J. Phys. Chem. A* **2009**, *113* (11), 2446–2455.
(47) Infante, I.; Raab, J.; Lyon, J. T.; Liang, B.; Andrews, L.; Gagliardi, L. *J. Phys. Chem. A* **2007**, *111* (47), 11996–12000.
(48) Boys, S. F.; Bernardi, F. *Mol. Phys.* **1970**, *19* (4), 553.
(49) Engkvist, O.; Åstrand, P. O.; Karlström, G. *Chem. Rev.* **2000**, *100* (11), 4087–4108.
(50) Brdarski, S.; Karlstrom, G. *J. Phys. Chem. A* **1998**, *102* (42), 8182–8192.
(51) Karlstrom, G. *Theor. Chim. Acta* **1982**, *60*, 535.
(52) Stace, A. J.; Walker, N. R.; Firth, S. *J. Am. Chem. Soc.* **1997**, *119* (42), 10239–10240.
(53) Corongiu, G.; Clementi, E. *J. Chem. Phys.* **1978**, *69* (11), 4885–4887.
(54) Jeanvoine, Y.; Spezia, R. *J. Mol. Struct. (Theochem)* **2010**, *954* (1−3), 7–15.
(55) Jeanvoine, Y.; Spezia, R. *J. Phys. Chem. A* **2009**, *113* (27), 7878–7887.
(56) Blades, A. T.; Jayaweera, P.; Ikonomou, M. G.; Kebarle, P. *J. Chem. Phys.* **1990**, *92* (10), 5900–5906.
(57) Jayaweera, P.; Ikonomou, M. G.; Kebarle, P. I. J. M. S. *Int. J. Mass Spectrom. Ion Processes* **1990**, *101*, 325.
(58) Blades, A. T.; Jayaweera, P.; Ikonomou, M. G.; Kebarle, P. *Int. J. Mass Spectrom., Ion Processes* **1990**, *102*, 251.
(59) El-Nahas, A. M.; Tajima, N.; Hirao, K. *Chem. Phys. Lett.* **2000**, *318* (4−5), 333–339.
(60) El-Nahas, A. M.; El-Demerdash, S. H.; El-Shereefy, E. S. E. *Int. J. Mass Spectrom.* **2007**, *263* (2−3), 267–275.
(61) Bush, M. F.; Saykally, R. J.; Williams, E. R. *J. Am. Chem. Soc.* **2008**, *130* (28), 9122–9128.
(62) Wu, J. C.; Piquemal, J. P.; Chaudret, R.; Reinhardt, P.; Ren, P. Y. *J. Chem. Theory Comput.* **2010**, *6* (7), 2059–2070.
(63) Linse, P.; Wallqvist, A.; Astrand, P. O.; Nymand, T. M.; Lobaskin, V.; Carlson, F. *Molsim*; Lund University: Sweden, 2003.
(64) Kolafa, J.; Perram, J. *Mol. Simul.* **1992**, *9*, 351.
(65) Joung, I. S.; Cheatham, T. E. *J. Phys. Chem. B* **2008**, *112* (30), 9020–9041.
(66) Jensen, K. P.; Jorgensen, W. L. *J. Chem. Theory Comput.* **2006**, *2* (6), 1499–1509.
(67) Darden, T.; Pearlman, D.; Pedersen, L. G. *J. Chem. Phys.* **1998**, *109* (24), 10921–10935.
(68) Warren, G. L.; Patel, S. *J. Chem. Phys.* **2007**, *127* (6), 064509.
(69) Rajamani, S.; Ghosh, T.; Garde, S. *J. Chem. Phys.* **2004**, *120* (9), 4457–4466.
(70) Carlsson, J.; Aqvist, J. *J. Phys. Chem. B* **2009**, *113* (30), 10255–10260.
(71) Gladich, I.; Shepson, P.; Szleifer, I.; Carignano, M. *Chem. Phys. Lett.* , *489* (1−3), 113–117.
(72) Kowall, T.; Foglia, F.; Helm, L.; Merbach, A. E. *J. Phys. Chem.* **1995**, *99* (35), 13078–13087.
(73) Kowall, T.; Foglia, F.; Helm, L.; Merbach, A. E. *J. Am. Chem. Soc.* **1995**, *117* (13), 3790–3799.
(74) Terrier, C.; Vitorge, P.; Gaigeot, M.-P.; Spezia, R.; Vuilleumier, R. *J. Chem. Phys.* **2010**, *133*, 044509.
(75) Buzko, V.; Sukhno, I.; Buzko, M. *Int. J. Quantum Chem.* **2007**, *107* (13), 2353–2360.
(76) Kuta, J.; Clark, A. E. *Inorg. Chem.* **2010**, *49* (17), 7808–7817.
(77) Allen, P. G.; Bucher, J. J.; Shuh, D. K.; Edelstein, N. M.; Craig, I. *Inorg. Chem.* **2009**, *39*, 595–601.
(78) Ruas, A.; Guilbaud, P.; Den Auwer, C.; Moulin, C.; Simonin, J. P.; Turq, P.; Moisy, P. *J. Phys. Chem. A* **2006**, *110* (41), 11770–11779.

JP105590H